FULL PAPER

Understanding Lattice Strain-Controlled Charge Transport in Organic Semiconductors: A Computational Study

Xiaoyan Zheng, Hua Geng, Yuanping Yi, Qikai Li, Yuqian Jiang, Dong Wang,* and Zhigang Shuai*

The softness and anisotropy of organic semiconductors offer unique properties. Recently, solution-sheared thin-films of 6,13-bis(triisopropylsilylethynyl) pentacene (TIPS-P) with nonequilibrium single-crystal domains have shown much higher charge mobilities than unstrained ones (*Nature* 2011, *480*, 504). However, to achieve efficient and targeted modulation of charge transport in organic semiconductors, a detailed microscopic understanding of the structure–property relationship is needed. In this work, motivated by the experimental studies, the relationship between lattice strain, molecular packing, and charge carrier mobility of TIPS-P crystals is elucidated. By employing a multiscale theoretical approach combining nonequilibrium molecular dynamics, first-principles calculations, and kinetic Monte Carlo simulations using charge-transfer rates based on the tunneling enabled hopping model, charge-transport properties of TIPS-P under various lattice strains are investigated. Shear-strained TIPS-P indeed exhibits one-dimensional charge transport, which agrees with the experiments. Furthermore, either shear or tensile strain lead to mobility enhancement, but with strong charge-transport anisotropy. In addition, a combination of shear and tensile strains could not only enhance mobility, but also decrease anisotropy. By combining the shear and tensile strains, almost isotropic charge transport could be realized in TIPS-P crystal with the hole mobility improved by at least one order of magnitude. This approach enables a deep understanding of the effect of lattice strain on charge carrier transport properties in organic semiconductors.

1. Introduction

Electronic and optoelectronic devices based on solution-processed organic thin-films are being driven by ease of fabrication, low-cost, large-area, and mechanical flexibility.[1–7] However, for practical applications, charge carrier mobilities of organic polycrystalline thin-films still await to be greatly improved. Charge transport properties of solution-processed polycrystalline thin-films are essentially determined by the morphology and molecular packing in single-crystalline domains. Several solution-processing techniques including air-flow,[8,9] roll-transfer printing,[10] solvent additives,[11] solvent and polymer matrix,[12] solution-shearing,[13,14] and fluid-enhanced crystal engineering[15] have been developed to align crystalline domains and improve the morphology of organic polycrystalline thin-films. Of these, the solution-shearing method has been proved to not only induce the grain alignment in polycrystalline thin-films, but also allow access of metastable non-equilibrium molecular packing motifs under shear strains.[14,15] 6,13-bis(triisopropylsilylethynyl) pentacene (TIPS-P) is an excellent hole transport material with great air stability.[16] Bao and co-workers reported that solution-sheared TIPS-P thin-film transistors show much higher hole mobilities than unstrained ones.[14,15] Controlling morphology at the same time of solution shearing poses several challenges. The most difficult one is to prevent crystal defects during film formation. These difficulties were recently to a large extent surpassed by engineering the fluid flow to control crystal nucleation and growth, and changing other processing conditions such as lowering the solution concentration and shearing speed.[15] The fabricated thin-films of TIPS-P show an unprecedented average and maximum mobilities of 8.1 ± 1.2 cm^2 V^{-1} s^{-1} and 11 cm^2 V^{-1} s^{-1},[15] which is a very encouraging result.

In organic crystalline materials, molecules are loosely bonded by van der Waals forces, so organic semiconductors are soft and feature anisotropic properties. For this reason, both shear and uniaxial strains can be applied to induce molecular packing reorganization and thus to modulate charge transport

X. Y. Zheng, Y. Q. Jiang, Dr. D. Wang, Prof. Z. G. Shuai
MOE Key Laboratory of Organic Optoelectronics
and Molecular Engineering
Department of Chemistry
Tsinghua University
100084, Beijing, P. R. China
E-mail: dong913@tsinghua.edu.cn;
zgshuai@tsinghua.edu.cn
Dr. H. Geng, Prof. Y. P. Yi
Key Laboratory of Organic Solids
Beijing National Laboratory for Molecular Science (BNLMS)
Institute of Chemistry
Chinese Academy of Sciences
100190, Beijing, P. R. China
Dr. Q. K. Li
School of Materials Science & Engineering
Tsinghua University
100084, Beijing, P. R. China

FULL PAPER

in organic semiconductors. However, efficient and targeted modulation of charge transport properties remains challenging. It needs a detailed microscopic understanding of the structure-property relationship. In other words, it is critical to know in which direction and to what extent shear and uniaxial strains should be applied in order to achieve enhanced charge carrier mobility. Recently developed touch-sensitive "electronic skin" that integrated organic thin-film transistors (OTFTs), pressure-sensitive sensors and organic light emitting diodes (OLEDs) over large-area and flexible substrate,[17,18] also raises questions on device response under pressure.[19–22]

In this work, inspired by the recent experimental advances, we seek to elucidate the relationship between lattice strain, molecular packing, and charge carrier mobility in TIPS-P crystals. We employ a multi-scale theoretical approach combining nonequilibrium molecular dynamics (NEMD) simulations, first-principles calculations, and kinetic Monte Carlo simulations using charge transfer rates based on the tunneling enabled hopping model, to investigate charge transport properties of TIPS-P under various lattice strains. The multi-scale protocol, which maps molecular packing at the atomistic level to charge transport at the mesoscopic scale, enables a deep understanding of the effect of lattice strain on charge transport properties in organic semiconductors.

By comparing our simulations to the solution-shearing experiments,[14,15] we glean insight into the overall charge transport properties of shear-strained TIPS-P crystals and explain the experimental observations successfully. On top of that, we

are able to predict charge transport behaviors of TIPS-P crystal under other types of lattice strains that are beyond access of current solution-shearing experiments. Finally, we propose an effective and delicate design of lattice-strained TIPS-P crystals with high mobility and low anisotropy.

2. Methodology

2.1. Model Setup

The unit-cell parameters of TIPS-P crystal with a = 7.80 Å, b = 7.82 Å, c = 17.00 Å, α = 103.3°, β = 88.1°, γ = 98.7° (**Scheme 1**a) are from the annealed sample prepared at shearing speed 8 mm s^{-1} in the experiment.[14] For the brick-wall packing TIPS-P, the dominant charge transport channels locate in the ab plane, with dimer T1 stacking along the b-axis, which corresponds to the shearing direction in the experiment[14] (Scheme 1b). The triclinic supercell of TIPS-P with size $10 \times 10 \times 3$ in the a, b, and c dimensions is constructed by a replication of the original unit cell, and it is used as the initial configuration for the MD simulations. The supercell is oriented in the Cartesian coordinate system with a along x and b in the xy plane (Scheme 1c). To tune the molecular packing of TIPS-P crystal in the ab plane, we consider four types of lattice strains: shear strain along the (+)xy or (−)xy direction and normal strain along the (+)xx or (−)xx direction (Scheme 1d).
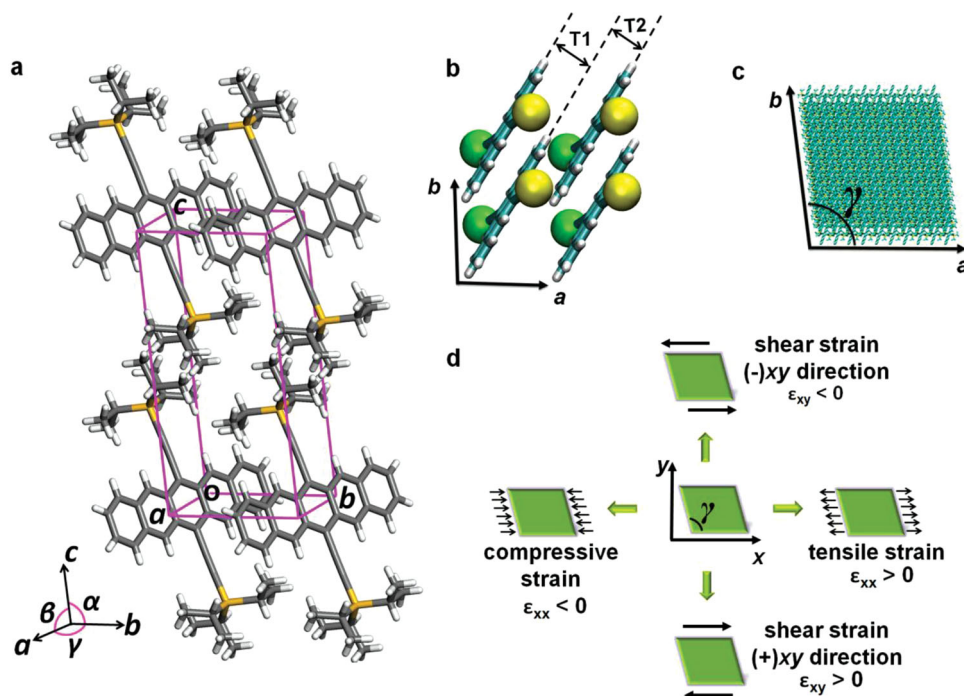

Scheme 1. a) Unit cell of TIPS-P crystal with a = 7.80 Å, b = 7.82 Å, c = 17.00 Å, α = 103.3°, β = 88.1°, γ = 98.7°. b) T1 and T2 represent two non-equivalent dimers in the ab plane of brick-wall packing TIPS-P crystal. The transfer integrals of dimers T1 and T2 are denoted by V1 and V2, respectively. c) Initial configuration of TIPS-P crystal for use in the MD simulations, with size $10 \times 10 \times 3$ in the a, b, and c dimensions generated by a replication of the original unit cell. The TIPS-P supercell is oriented in the Cartesian coordinate system with a along x and b in the xy plane. d) Definition of four types of lattice strains applied in NEMD simulations: normal strain ε_{xx} along the (+)xx direction (tensile, $\varepsilon_{xx} > 0$) and (−)xx direction (compressive, $\varepsilon_{xx} < 0$); shear strain ε_{xy} along the (+)xy direction ($\varepsilon_{xy} > 0$) and (−)xy direction ($\varepsilon_{xy} < 0$). In the (+)xy direction γ decreases, while in the (−)xy direction γ increases in the shearing process. Note that the symbols "+" and "−" represent lattice strain directions only, the magnitude of lattice strain is measured by $|\varepsilon_{xx}|$ and $|\varepsilon_{xy}|$.

Materials Views
www.MaterialsViews.com

ADVANCED
FUNCTIONAL
MATERIALS
www.afm-journal.de

FULL PAPER

2.2. MD Simulations

All MD simulations are performed by using the LAMMPS software package.[23] The atom types and interaction parameters of TIPS-P are built from the general Amber force field (GAFF),[24] which is a well-established force field for organic small molecules. The electrostatic potential of TIPS-P molecule is calculated by the HF/6–31G* method using the Gaussian 09 package,[25] and the partial charge on each atom that reproduces the overall electrostatic potential distribution is obtained by the restrained electrostatic potential (RESP) fitting method.[26,27] Periodic boundary conditions are applied in all three dimensions to minimize the edge effects in a finite system. The cutoff for the van der Waals interactions is set to 10.0 Å. The time step used to integrate the equation of motion is 1 fs. The pressure and temperature of the system is controlled by using the Nosé-Hoover thermostat and barostat[28,29] at 1 K and zero atm. The thermostat and barostat relaxation times are set to 10 and 1000 fs, respectively. The initial supercell structure with size $10 \times 10 \times 3$ in the a, b, and c dimensions constructed from the experimental parameters,[14] as described above, is first energy minimized and then relaxed for 100 ps in the NPT ensemble. The relaxed triclinic supercell has the size of 77.000 Å × 75.450 Å × 50.271 Å, with $\alpha = 106.471°$, $\beta = 85.820°$, $\gamma = 96.463°$, respectively, which is hereafter referred to as the unstrained TIPS-P in this work.

Next, starting from the unstrained TIPS-P supercell, several NEMD simulations at 1 K are performed to impose different types of lattice strains on it. During each NEMD simulation, the unstrained TIPS-P crystal is strained in a designated direction with a constant strain rate of 1×10^7 s^{-1}, and the strain is applied every time step, meanwhile, the stress components in all other directions are controlled and always kept zero. As such, the simulated supercell is allowed to relax in both size and shape in each direction independently. In this way, we can release the stress induced in non-strained directions, which makes the mechanical properties of molecular crystals calculated from 1D stress-strain curves more reliable. The TIPS-P crystal is only lattice-strained in the ab plane, in which the main charge transport pathways locate. The NEMD simulations were performed as follows: i) Apply shear strain on the unstrained TIPS-P along the $(+)xy$ and $(-)xy$ directions, respectively, with ε_{xy} changing from 0 to 0.09 and 0 to -0.1 at a constant rate of 10^7 s^{-1}. The TIPS-P structural parameters are extracted from the MD trajectories at a shear strain interval of 0.01, and used for the subsequent hole mobility calculations; ii) Impose normal strain on the unstrained TIPS-P along the $(+)xx$ and $(-)xx$ directions, respectively, with ε_{xx} changing from 0 to 0.13 and 0 to -0.03 at a constant rate of 10^7 s^{-1}. The TIPS-P structural parameters are extracted from the MD trajectories at a normal strain interval of 0.01, and used for the subsequent hole mobility calculations; iii) Impose an extra shear strain ε_{xy} along the $(+)xy$ and $(-)xy$ directions, respectively, on the normal-strained crystal obtained in the second step, with ε_{xy} changing from 0 to 0.05 and 0 to -0.1 at a constant rate of 10^7 s^{-1}. And the previously imposed normal strain is kept fixed in this step. Again, the TIPS-P structural parameters are extracted from the MD trajectories at a shear strain interval of 0.01 for the subsequent hole mobility calculations. As can be seen below, all the lattice strains applied here are within the elastic regime of the stress-strain curves (**Figure 1**). Since the NEMD simulations
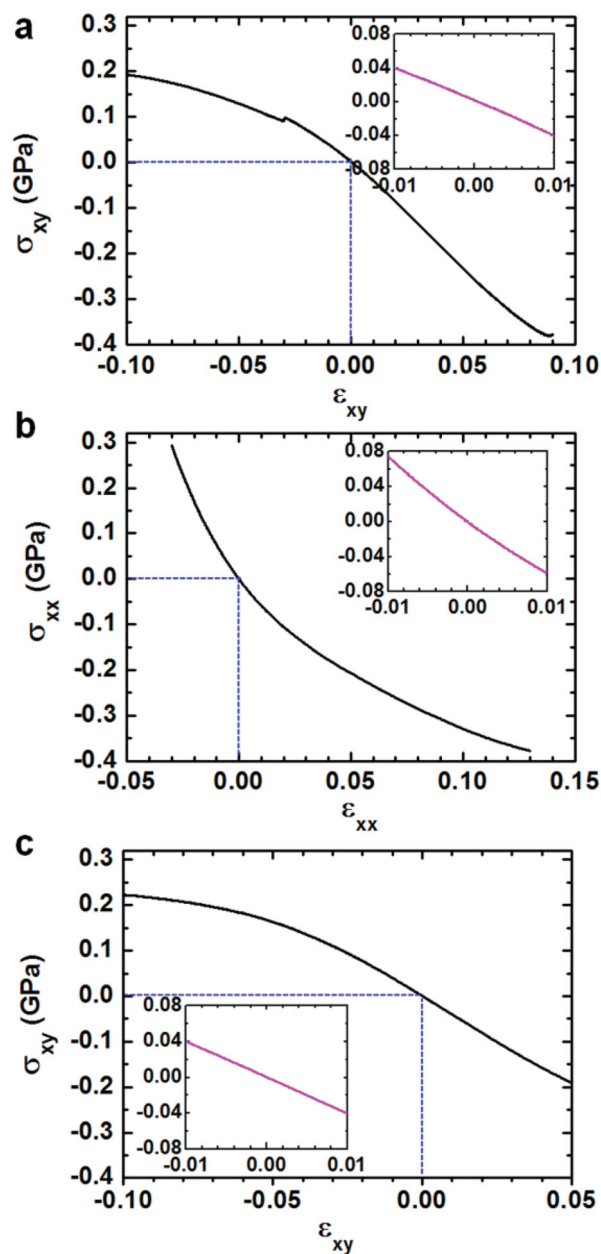
Figure 1. Stress–strain curves within the elastic regime from the NEMD simulations of TIPS-P crystals. a) Shear strain along both the $(+)xy$ and $(-)xy$ directions. b) Normal strain along both the $(+)xx$ and $(-)xx$ directions. c) Shear strain along both the $(+)xy$ and $(-)xy$ directions with tensile strain fixed at $\varepsilon_{xx} = 0.13$. The linear elastic regime of each stress-strain curve with lattice strain in the range of ±0.01 is shown in the inset.

are performed at 1 K, the molecules in the supercell remain ordered and we simply extract the TIPS-P unit-cell parameters from the parameters and size of the supercell.

2.3. Mobility Calculations

Given the lattice-strained unit-cell parameters extracted from the above-mentioned NEMD simulations, we calculate the

charge carrier mobility of lattice-strained TIPS-P crystals. It is noted that the reorganization energy λ is not affected by lattice strains. It is 217 meV evaluated by the normal-mode analysis method,[30,31] and is close to 222 meV calculated by the adiabatic potential energy surface method,[32,33] suggesting that the harmonic oscillator approximation is successful. The intermolecular transfer integral V is calculated by the site-energy overlap correction method.[34] For TIPS-P with $\lambda \gg V$, the charge transport can be well modeled by the hopping mechanism. The charge carrier mobility is predicted by the first-principles calculations of molecular parameters coupled with charge transfer rate theory and a random walk simulation.[35–37] Here, we describe intermolecular charge carrier hopping behavior by a full-quantum charge transfer rate,[36,37] which has been shown to exhibit quantum nuclear tunneling effect, and such effect has been confirmed experimentally.[38] As mentioned earlier, the brick-wall packing TIPS-P exhibits two-dimensional (2D) charge transport in the ab plane. We then use the lattice-strained unit-cell parameters to re-construct a lattice-strained supercell with size $60 \times 60 \times 1$ in the a, b, and c dimensions for the kinetic Monte Carlo simulations of charge carrier diffusion. Neither the fluctuation of transfer integral nor that of site energy is considered here, because in the current investigation we focus on charge transport modulated by lattice strains. More details about the charge carrier mobility calculation methods are provided in the Supporting Information (SI).

3. Results and Discussion

3.1. Stress–Strain Relationship

The elastic modulus of organic materials is usually smaller than the conventional materials, such as inorganic semiconductors and ordinary metals, by about one order of magnitude. So the molecular packing of organic semiconductors can be effectively modified by moderate external pressure, to show dramatic changes in charge transport properties.

All the stress-strain curves obtained from the NEMD simulations (Figure 1) are within the elastic regime before the yield point. The linear elastic regime only exists at very low lattice strain of each stress-strain curve (see Figure 1 inset). The elastic modulus obtained by the least-squares fitting of each curve within the linear elastic regime in Figure 1a-c is 4.0 GPa for pure shear strain, 6.7 GPa for pure normal strain, and 4.0 GPa for combined shear and normal strains. These figures are much smaller than those of graphene (~2.0 TPa),[39] carbon nanotubes (~1.2 TPa),[40] and ordinary steels (~100–300 GPa). The elastic modulus of a material determines how much it will strain under a given amount of external stress. The larger the elastic modulus, the stiffer the material is. Thus, straining TIPS-P crystal along the xy direction is easier than along the xx direction. In the nonlinear elastic regime, i) for either pure shear-strained TIPS-P (Figure 1a) or extra shear strain applied on normal-strained TIPS-P (Figure 1c), the shear response in the (–)xy direction is parabolic, and the slope of the curve decreases with increasing $|\varepsilon_{xy}|$, while in the (+)xy direction, the shear response is almost linear; ii) the normal responses to both compression and tension along the xx direction are

parabolic (Figure 1b), and as tensile strain increases, the slope of the curve decreases while as compressive strain increases, the slope of the curve increases. Overall, the stress-strain relationship shows that TIPS-P crystal under shear stress in the (–)xy direction or tensile stress in the (+)xx direction undergoes easier deformation.

3.2. Charge Transport Properties under Lattice Strains

We first confirm that the lattice-strained TIPS-P crystals in the experiment correspond to shear-strained ones along the (–)xy direction in our simulation. The unit-cell parameters in the ab plane as a function of shear strain ε_{xy} along the (–)xy direction are shown in **Figure 2**a. During this shearing process, a decreases from 7.70 Å to 7.51 Å, concurrently b increases from 7.55 Å to 8.10 Å and γ also increases. Owing to the Poisson's effect, β also changes slightly, but c and α remain almost unchanged. Thus, deformation mainly occurs in the ab plane and the unit-cell shape becomes more oblique, which qualitatively resemble the experimental measurement of the unit-cell parameters as a function of shearing speed (see Supplementary Table 1 in Ref.[14] and Figure S1 in SI). At the same time, transfer integral $V1$ increases from 2.6 meV to 40.9 meV, and $V2$ remains almost unchanged (Figure 2b), so the difference between $V1$ and $V2$ enlarges, which indicates larger charge transport anisotropy. The shear-strained TIPS-P crystal indeed shows 1D charge transport mainly along the b-axis, which agrees with the experimental observation that the hole mobility parallel to the shearing direction was higher than perpendicular.[14] As $|\varepsilon_{xy}|$ increases, the hole mobility along the b-axis, μ^b, increases from 0.31 cm² V⁻¹ s⁻¹ for the unstrained TIPS-P to 7.0 cm² V⁻¹ s⁻¹ for the shear-strained TIPS-P at $\varepsilon_{xy} = -0.09$, and the in-plane average hole mobility μ^{avg} increases from 0.34 cm² V⁻¹ s⁻¹ to 3.7 cm² V⁻¹ s⁻¹ accordingly (Figure 2c). In the experiment,[14] the hole mobility increased from 0.8 cm² V⁻¹ s⁻¹ for unstrained films up to as high as 4.6 cm² V⁻¹ s⁻¹ in shear-strained thin films. Both our simulation and the solution-shearing experiments[14,15] disclose increasingly oblique unit-cell geometry and 1D charge transport behavior along the b-axis in shear-strained TIPS-P crystals. In the solution shearing experiment, when the applied shearing speed was higher, the unit-cell shape identified in single-crystal domains became more oblique, and such a molecular packing favored charge transport along the elongated crystallite growth direction.[14] However, due to the formation of smaller and less oriented crystallites, which introduce more grain boundaries with less electronic couplings, the experimentally observed mobilities decreased sharply when the shearing speed was higher than 2.8 mm s⁻¹.[14] So, although shear strain offers an effective approach for modulation of charge transport in organic semiconductors, controlling the growth of non-equilibrium single-crystalline domains by solution-processing techniques remains challenging. Bao and co-workers reported that engineering the fluid flow at the same time of solution shearing at a lower shearing speed and a lower solution concentration is able to attain not only controlled morphology but also controlled molecular packing. The average hole mobility of their single-crystalline TIPS-P thin-films finally reached 8.1 ± 1.2 cm² V⁻¹ s⁻¹, and the maximum hole mobility was as

www.MaterialsViews.com

**ADVANCED
FUNCTIONAL
MATERIALS**
www.afm-journal.de

FULL PAPER
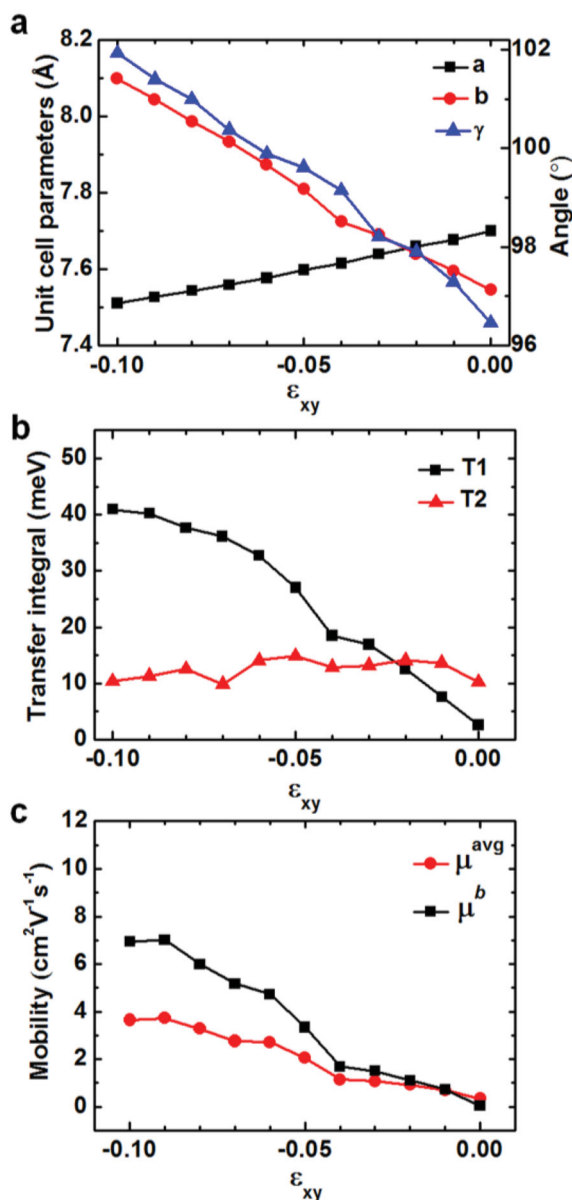
Figure 2. a) Unit-cell parameters *a*, *b*, and *γ* in the *ab* plane as a function of shear strain ε_{xy} along the (−)*xy* direction extracted from the NEMD simulations. b) Transfer integrals *V*1 and *V*2 for dimers T1 and T2. c) in-plane average hole mobilities μ^{avg} and hole mobilities along the *b*-axis, μ^{b}.

high as 11 cm² V⁻¹ s⁻¹.[15] We need to point out that our NEMD simulations cannot be directly related to the solution shearing experiment, in which the molecular packing changes as a function of shearing speed. In the simulations, the strain rate is usually too high for the effect of shearing speed to be observed. But the trend of change in unti-cell parameters extracted from the above shearing simulation and the corresponding hole mobilities are consistent with those reported experimentally.

By comparison with and a reasonable explanation of the experimental result, our multi-scale theoretical protocol is validated. Furthermore, we are able to predict charge transport properties of TIPS-P crystals under other types of designed lattice strains, which are at the moment beyond the access of
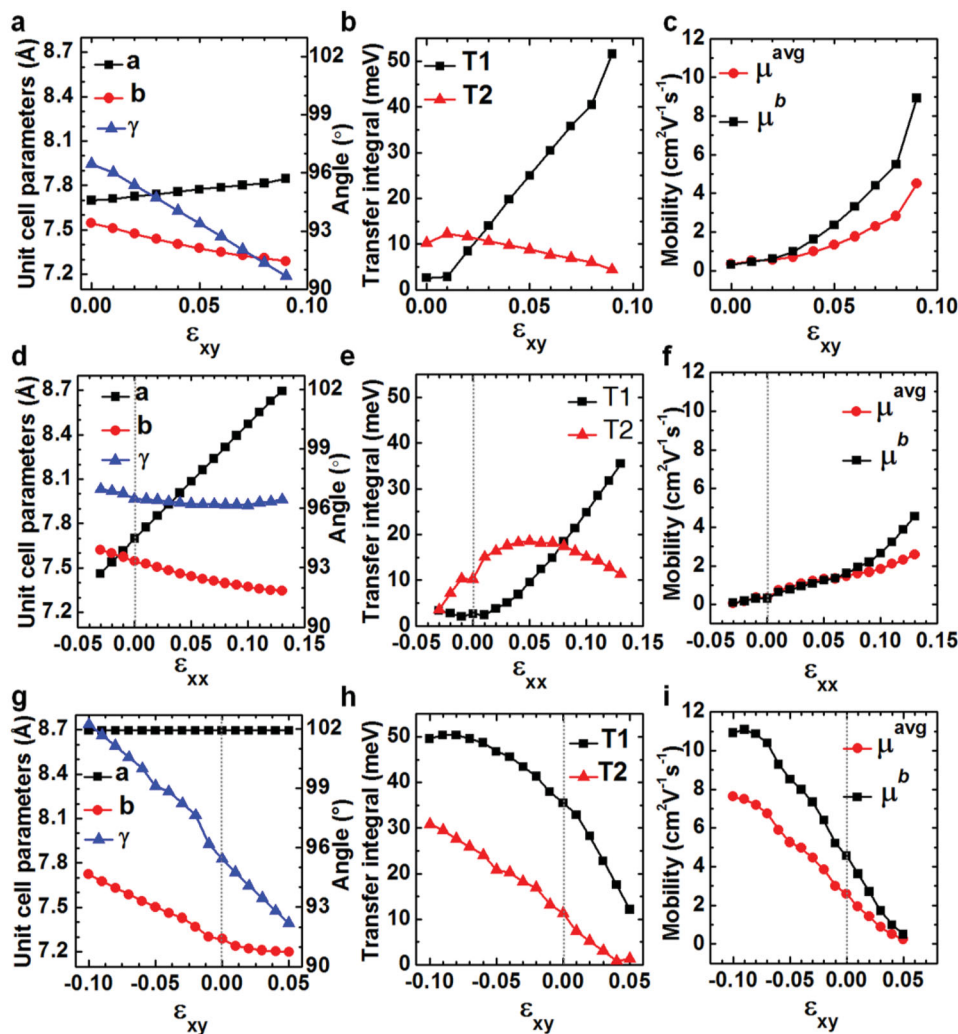
solution-shearing experiment. When shear strain is imposed along the (+)*xy* direction, the in-plane unit-cell geometry becomes less oblique, opposite to that when shear strain is along the (−)*xy* direction, but the charge transport behavior is similar, irrespective of the shearing direction (**Figure 3**a–c). When shearing along the (+)*xy* direction, *V*1 increases monotonically, while *V*2 decreases, as a result, the charge transport anisotropy enlarges. It is amazing to see that, no matter in which direction shear strain is applied, transfer integral *V*1 along the *b*-axis always increases with $\left|\varepsilon_{xy}\right|$. It indicates that shear-strained TIPS-P crystals always exhibit 1D charge transport behavior along the *b*-axis. The μ^{b} for shear-strained TIPS-P at $\varepsilon_{xy} = 0.09$ reaches 8.9 cm² V⁻¹ s⁻¹.

When uniaxial (normal) strain along the *xx* direction is imposed, only *a* shows obvious change, other unit-cell parameters remain almost unchanged (Figure 3d). For compressed TIPS-P, both *V*1 and *V*2 are small, leading to low charge carrier mobility. When tensile strain is applied, with ε_{xx} increasing from 0 to 0.13, *V*1 increases and *V*2 first increases then decreases (Figure 3e). Consequently, μ^{b} increases to 4.6 cm² V⁻¹ s⁻¹ for tensile-strained TIPS-P (Figure 3f). Both μ^{b} and μ^{avg} of normal-strained TIPS-P are smaller than those of shear-strained TIPS-P, and the charge transport anisotropy is also lower.

After a thorough investigation of charge transport properties of TIPS-P under pure shear and pure normal strain in a desired directioin, we consider combination of shear and normal strains. With normal strain fixed at $\varepsilon_{xx} = 0.13$, shear strain along the (+)*xy* and (−)*xy* directions, respectively, is applied. During the shearing process, *a* remains constant and other unit-cell parameters undergo changes similar to those of pure shear-strained TIPS-P (see Figures 2a, 3a and 3g). It is exciting to see that, as $\left|\varepsilon_{xy}\right|$ along the (−)*xy* direction increases, both *V*1 and *V*2 increase, so the charge transport anisotropy is lower than that of pure shear-strained TIPS-P, and the maximum μ^{b} and μ^{avg} obtained are 11 cm² V⁻¹ s⁻¹ and 7.7 cm² V⁻¹ s⁻¹, respectively (Figure 3h-i). It shows that combining shear and normal strains offers an efficient way for tailoring molecular packing in organic semiconductors to attain high mobility and low charge transport anisotropy. The unit-cell parameters of all lattice-strained TIPS-P crystals mentioned above have been summarized in Tables S1–3 and Tables S9–24 in SI.

3.3. Understanding Structure–Property Relationships

The electronic coupling strength is represented by the intermolecular transfer integral, which is intimately related to the overlap between adjacent molecular orbitals and is a key parameter influencing charge transport in organic semiconductors. The transfer integral is sensitive to the relative position and orientation of adjacent molecules, as shown earlier by Brédas et al.[41] And in general, a subtle change in the molecular packing parameters may induce a dramatic change of charge carrier mobility. To elucidate the structure-property relationship in TIPS-P crystals, we scrutinize the effect of two major types of intermolecular motions, experienced in the straining process, on the transfer integrals: i) π–π stacking distance $d_{\pi-\pi}$ and ii) molecular displacements along the long and short axes, d_{long} and d_{short}. The definition of the molecular long and short axes
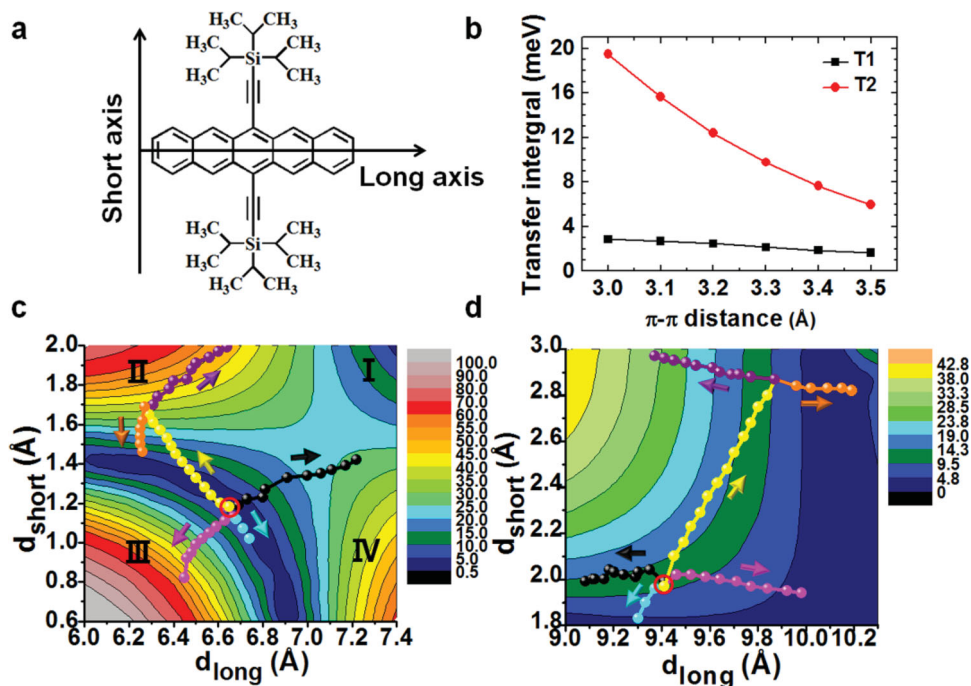
FULL PAPER

ADVANCED
FUNCTIONAL
MATERIALS
www.afm-journal.de

Materials
Views
www.MaterialsViews.com

Figure 3. Unit-cell parameters in the *ab* plane and charge transport properties of TIPS-P crystals under designed lattice strains. a, b, c) Unit-cell parameters, transfer integrals *V1* and *V2* for dimers T1 and T2, in-plane average hole mobilities μ^{avg} and hole mobilities along the *b*-axis μ^b of shear-strained TIPS-P along the (+)*xy* direction. d, e, f) Unit-cell parameters, transfer integrals and hole mobilities of normal-strained TIPS-P along the *xx* direction for both uniaxial compression and tension. g, h, i) Unit-cell parameters, transfer integrals, and hole mobilities of shear-strained TIPS-P along the (−)*xy* and (+)*xy* directions with normal strain fixed at $\varepsilon_{xx} = 0.13$.

in TIPS molecule is shown in **Figure 4**a. The molecular packing parameters $d_{\pi-\pi}$, d_{long} and d_{short} of lattice-strained TIPS-P crystals investigated above have been summarized in Tables S4–6 in SI. It is observed that, i) during the straining process, $d_{\pi-\pi}$ changes much less than d_{long} and d_{short}; ii) when $d_{\pi-\pi}$ decreases, the transfer integral does not necessarily increase, instead, it is more sensitive to molecular displacements along the long and short axes d_{long} and d_{short}.

To understand the lattice strain controlled charge transport in TIPS-P crystal, intermolecular transfer integrals are scanned in the space of molecular packing parameters $d_{\pi-\pi}$, d_{long} and d_{short}. Figure 4b illustrates the evolution of *V1* and *V2* as a function of $d_{\pi-\pi}$, with both d_{long} and d_{short} of dimers T1 and T2 fixed at those measured for the unstrained TIPS-P crystal. It is not surprising to see that the magnitude of both *V1* and *V2* decays with increasing $d_{\pi-\pi}$, due to the reduced overlap of molecular orbitals when adjacent molecules are separated apart. Moreover,

with both d_{long} and d_{short} fixed, transfer integrals change at most 15 meV when $d_{\pi-\pi}$ varies by 0.5 Å, and the absolute value of *V1* is always less than that of *V2* as seen in the unstrained TIPS-P. Figure 4c-d illustrates the evolution of *V1* and *V2* as a function of d_{long} and d_{short} respectively, with $d_{\pi-\pi}$ of dimers T1 and T2 respectively fixed at the value measured for unstrained TIPS-P crystal. For dimer T1, the entire contour plot (Figure 4c) can be divided into four regions labeled as I-IV based on the cross-shaped zone in cyan color.

Then, the d_{long} and d_{short} of lattice-strained TIPS-P crystals (see Tables S4–6) obtained from the NEMD simulations are mapped onto the contour plots of Figure 4c-d, which constitute the lattice-strain pathways along different directions. It is clear that the most prominent increase of transfer integrals is identified to be along the pure shear strain pathway in the (+)*xy* direction (*magenta*) and the one in the (−)*xy* direction with normal strain fixed at $\varepsilon_{xx} = 0.13$ (*purple*). With pure shear strain

Materials
Views
www.MaterialsViews.com

ADVANCED
FUNCTIONAL
MATERIALS
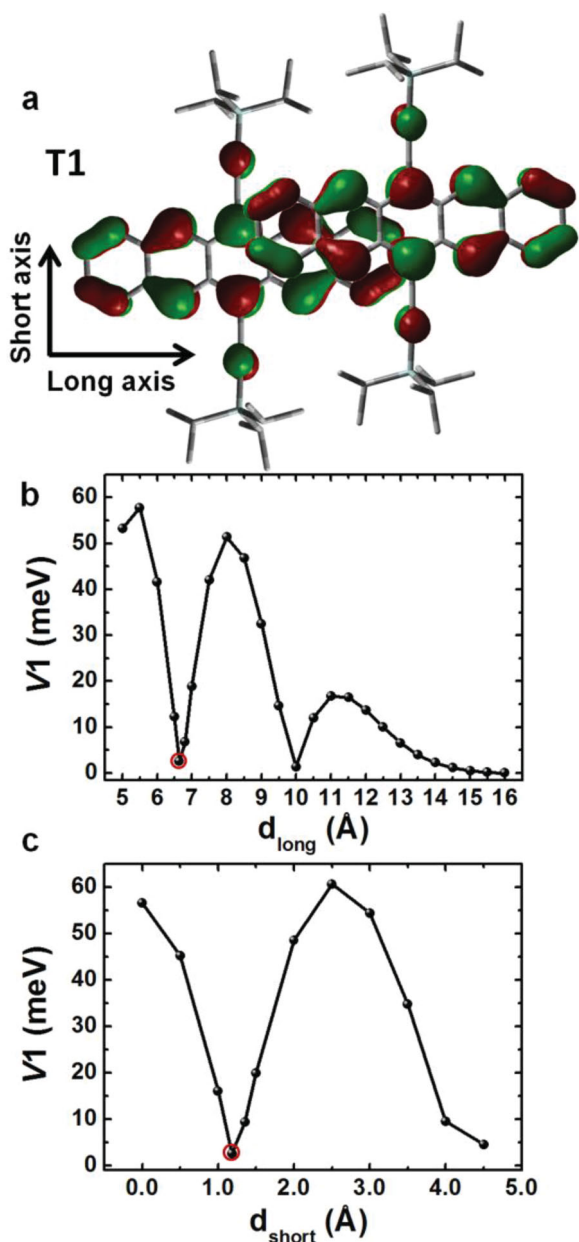www.afm-journal.de

FULL PAPER

Figure 4. Relationship between molecular packing and intermolecular transfer integrals of TIPS-P crystals. a) Definition of the long and short axes in TIPS-P molecule. b) Evolution of transfer integrals $V1$ and $V2$ as a function of the $\pi-\pi$ stacking distance $d_{\pi-\pi}$, with the molecular displacements along the long and short axes d_{long} and d_{short} fixed at the values measured for unstrained TIPS-P crystal obtained from the NPT simulation. c) 2D contour plot of transfer integral $V1$ (meV) projected onto d_{long} and d_{short}, with $d_{\pi-\pi}$ fixed at 3.367 Å, that of the unstrained TIPS-P crystal. The entire 2D contour plot is divided into four regions labeled as I-IV based on the cross-shaped zone in cyan color. d) 2D contour plot of transfer integral $V2$ (meV) as a function of d_{long} and d_{short}, with $d_{\pi-\pi}$ fixed at 3.282 Å, that of the unstrained TIPS-P crystal. The molecular packing parameters d_{long} and d_{short} of lattice-strained TIPS-P crystals obtained from the NEMD simulations are labeled by colored spheres in c and d: *black*, shear strain along the (−)xy direction; *magenta*, shear strain along the (+)xy direction; *cyan*, compressive strain along the (−)xx direction; *yellow*, tensile strain along the (+)xx direction; *purple*, shear strain along the (−)xy direction with normal strain fixed at $\varepsilon_{xx} = 0.13$; *orange*, shear strain along the (+)xy direction with normal strain fixed at $\varepsilon_{xx} = 0.13$. The location of the unstrained TIPS-P is marked by a red circle, from there the pure shear or normal strain is applied.

applied in the (+)xy direction, $V1$ increases by 49 meV and $V2$ decreases by 5.9 meV, leading to a reversal of the magnitude of $V1$ and $V2$ compared to the unstrained TIPS-P. As a result, such shear-strained TIPS-P features 1D charge transport along the b-axis. When shear strain is applied in the (−)xy direction with normal strain fixed at $\varepsilon_{xx} = 0.13$, both $V1$ and $V2$ increase, giving rise to higher charge carrier mobility and lower charge transport anisotropy. If shear strain is imposed directly in the (−)xy direction without normal strain (*black*), $V1$ increases by 38.3 meV and $V2$ remains almost unchanged. Obviously, modulating charge transport in TIPS-P by combined shear and normal strains is more efficient than by pure shear strains. Our results suggest that if accurate control of the direction and magnitude of shear and normal strains is achieved through solution-processing techniques, charge transport properties of TIPS-P will be further improved.

As demonstrated above, lattice strains lead to concurrent changes of molecular packing parameters $d_{\pi-\pi}$, d_{long} and d_{short}, which together are responsible for the intermolecular transfer integral changes. In the brick-wall packing TIPS-P, d_{long} and d_{short} seem to have larger impact on the intermolecular transfer integrals than $d_{\pi-\pi}$. A few tenths Å change of the molecular displacements leads to a few tens meV change of the transfer integrals. To illustrate how transfer integrals vary with d_{long} and d_{short}, the highest occupied molecular orbital (HOMO) of

TIPS-P molecules in dimer T1 is displayed in **Figure 5**a, and $V1$ changing as a function of d_{long} and d_{short}, is shown in Figure 5b-c respectively. We take dimer T1 in the unstrained TIPS-P as a reference, whose position in Figure 5b-c is labeled by a red circle, and displace one of the TIPS-P molecules along the long and short axes, respectively, over a distance much larger than that experienced in the NEMD simulations. When shifting the molecule along either the long or short axis, other molecular packing parameters are fixed at those of the unstrained TIPS-P.

It is apparent that $V1$ as a function of d_{long} and d_{short} is not monotonic, due to the complicated nodal structure of the HOMO orbital. Actually, $V1$ oscillates with the displacements along both the long and short axes, with a periodicity of 2.5 Å which corresponds largely to an aromatic ring size of TIPS-P.[41] Both the maxima and minima of $V1$ decrease with increasing d_{long} and d_{short}. When d_{long} is larger than 14 Å or d_{short} is larger than 4 Å, $V1$ nearly decays to zero. Large electronic coupling shows up when molecules interact in a fully bonding or fully anti-bonding fashion, and small electronic coupling occurs when there exists a cancellation between bonding and anti-bonding overlaps. The above analysis shows that the magnitude of transfer integrals is not only determined by molecular packing parameters $d_{\pi-\pi}$, d_{long} and d_{short}, but also by the nodal structure of frontier molecular orbitals, as demonstrated ealier by Brédas et al.[41]

ADVANCED
FUNCTIONAL
MATERIALS
www.afm-journal.de

FULL PAPER

www.MaterialsViews.com

Figure 5. a) HOMO orbital of TIPS-P molecules in dimer T1. b) Intermolecular transfer integral $V1$ as a function of d_{long}, with $d_{\pi-\pi}$ and d_{short} fixed at 3.367 Å and 1.183 Å, respectively, of unstrained TIPS-P from the NPT simulation. c) Intermolecular transfer integral $V1$ as a function of d_{short}, with $d_{\pi-\pi}$ and d_{long} fixed at 3.367 Å and 6.647 Å, respectively, of unstrained TIPS-P from the NPT simulation. The position of the unstrained TIPS-P is marked by a red circle in b and c.

### 3.4. Tuning Charge Transport by Combining Shear and Normal Strains

In summary, by combining ε_{xy} and ε_{xx} we obtain 272 lattice-strained TIPS-P crystals from the NEMD simulations, and investigate their charge transport properties. The unit-cell parameters (Table S3 and Tables S9–24) and intermolecular transfer integrals (Tables S7–8) of all the lattice-strained TIPS-P crystals are summarized in SI. The three-dimensional (3D)

plots of room temperature μ^{avg} and μ^b for all lattice-strained TIPS-P crystals as a function of ε_{xx} and ε_{xy} are demonstrated in **Figure 6**a and b, respectively. It shows that, in the tensile-strained region: i) with ε_{xx} fixed in between 0–0.13, when ε_{xy} along the (–)xy direction varies from 0 to –0.1, both μ^{avg} and μ^b increase monotonically; ii) with ε_{xx} fixed in between 0.05–0.13, when ε_{xy} along the (+)xy direction increases, both μ^{avg} and μ^b decrease, and with ε_{xx} fixed in between 0–0.04, an opposite trend is observed. Overall, the lattice-strained TIPS-P crystal with $\varepsilon_{xx} = 0.13$ and $\varepsilon_{xy} = -0.1$ exhibits the highest μ^{avg} and μ^b, which are 7.7 cm^2 V^{-1} s^{-1} and 11 cm^2 V^{-1} s^{-1}, respectively.

The anisotropy of charge carrier mobilities in lattice-strained TIPS-P crystals is also of interest. Figure 6c shows the angular-resolved hole mobilities in the unstrained and four lattice-strained TIPS-P crystals. The direction along the b-axis is denoted as 0°. The radius of dotted circles reflects the magnitude of mobility, and its magnitude can be read by projection at 0°/180° to the vertical axis shown on the left. So the dotted circles in Figure 6c represent hole mobilities ranging from 0 to 12 cm^2 V^{-1} s^{-1} at an interval of 1 cm^2 V^{-1} s^{-1}. It demonstrates that: i) Hole mobilities of lattice-strained TIPS-P crystals **2–5** are always higher than the unstrained TIPS-P crystal **1**; ii) Shear-strained TIPS-P crystals **2** ($\varepsilon_{xy} = -0.09$) and **3** ($\varepsilon_{xy} = 0.09$) show remarkably stronger charge transport anisotropy than tensile-strained TIPS-P crystal **4** ($\varepsilon_{xx} = 0.13$), with **3** exhibiting even stronger anisotropy than **2**. The maximum charge carrier mobilities in the ab plane are 6.6 cm^2 V^{-1} s^{-1}, 8.9 cm^2 V^{-1} s^{-1}, and 4.6 cm^2 V^{-1} s^{-1}, respectively, for **2**, **3**, and **4**, and the direction is along the b-axis for all of them; iii) Lattice-strained TIPS-P crystal **5** with combined shear and normal strains ($\varepsilon_{xx} = 0.13$ and $\varepsilon_{xy} = -0.1$) exhibits the highest mobility and the lowest charge transport anisotropy, with the maximum mobility in the ab plane being 12 cm^2 V^{-1} s^{-1} at 165°/345°; iv) The par/per ratios (ratios of mobilities parallel to and perpendicular to the b-axis) of TIPS-P crystals **1–5** are 0.8, 15, 122, 7.6 and 2.6, respectively. The experimentally identified par/per ratio for shear-strained TIPS-P crystal[15] was ~50, which agrees reasonably with our result for crystal **2** ($\varepsilon_{xy} = -0.09$). The most important finding here is that, by combining shear and normal strains we realize almost isotropic charge transport in TIPS-P, and the hole mobility is improved by at least one order of magnitude compared to the unstrained one.

4. Conclusion and Perspectives

The efficient and targeted control of molecular packing and charge transport in organic semiconductors poses a challenge to both experimentalists and theoreticians. Recent experimental reports of fabricating polycrystalline thin-films with non-equilibrium single-crystal domains represent an important step forward in this field. Charge carrier mobility of an air-stable and solution-processable p-type organic semiconductor, TIPS-P, has been reported to increase by an order of magnitude. The enhancement has two origins, one is the improved morphology of TIPS-P thin-films with aligned single-crystal domains, and the other is the non-equilibrium molecular packing that is benefitial for charge transport in certain directions. The lattice-strained single-crystalline domains with non-equilibrium
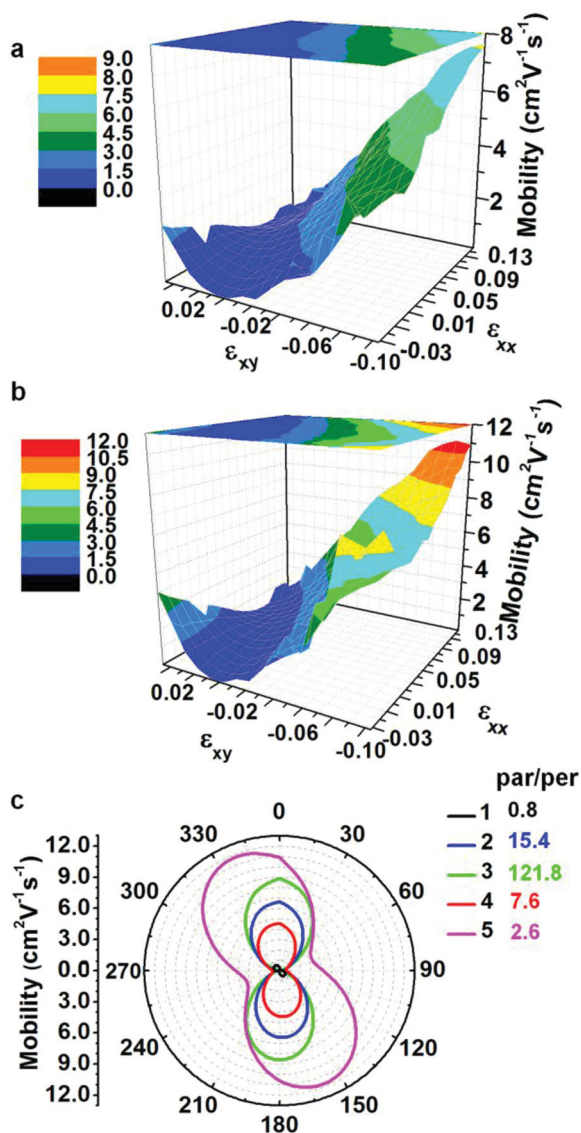
Figure 6. 3D plot of a) in-plane average mobility μ^{avg} and b) mobility along the b-axis μ^b for all 272 lattice-strained TIPS-P crystals as a function of ε_{xx} and ε_{xy}. c) Angular-resolved charge carrier mobilities in the ab plane of the unstrained and four lattice-strained TIPS-P crystals. The angle 0° represents the direction along the b-axis. The dotted circles correspond to mobilities between 0 and 12 cm^2 V^{-1} s^{-1} at an interval of 1 cm^2 V^{-1} s^{-1}. **1** black: unstrained TIPS-P from the NPT simulation; **2** blue: pure shear-strained TIPS-P with $\varepsilon_{xy} = -0.09$; **3** green: pure shear-strained TIPS-P with $\varepsilon_{xy} = 0.09$; **4** red: pure tensile-strained TIPS-P with $\varepsilon_{xx} = 0.13$; **5** magenta: combined lattice-strained TIPS-P with $\varepsilon_{xx} = 0.13$ and $\varepsilon_{xy} = -0.1$. The par/per denotes ratio of mobilities parallel to and perpendicular to the b-axis, shearing direction in the experiment,[15] for TIPS-P crystals.

molecular packing motifs have been shown to be thermodynamically metastable.[14,15] It is suggested to be a unique feature of soft and anisotropic organic crystalline materials, in which molecules are bonded together via weak non-covalent interactions. To effectively tune charge transport in organic semiconductors by lattice strains, a detailed microscopic understanding of the structure-property relationship of interested materials is needed.

In this work, charge transport properties of TIPS-P under various lattice strains are investigated by employing a multiscale theoretical approach, where nonequilibrium molecular dynamics simulations are performed to study the lattice-strain induced structural changes, first-principles calculations and kinetic Monte Carlo simulations are used to obtain the transfer integrals, reorganization energies and charge carrier mobilities. It is shown that shear-strained TIPS-P along the $(-)xy$ direction indeed exhibits 1D charge transport along the b-axis, which agrees with the experiment. We then study the effects of other types of strains and find that either shear or tensile strain leads to the mobility enhancement, but with strong charge transport anisotropy. Instead, a combination of shear and tensile strains could not only enhance the mobility, but also decrease the anisotropy. And we are able to realize almost isotropic charge transport in TIPS-P crystal with the hole mobility improved by at least one order of magnitude. The highest hole mobility attained for our lattice-strained TIPS-P crystals is 12 cm^2 V^{-1} s^{-1}, which is 39 times higher than 0.31 cm^2 V^{-1} s^{-1} for the unstrained TIPS-P crystal. These theoretical results suggest that, to push the limit of charge carrier mobility of a given material, accurate control of the strain direction and magnitude is a must. The theoretical predictions made in this work are expected to provide helpful guidance for the design of solution-shearing experiments.

In studying the effect of lattice strain on the intermolecular transfer integral, we find that the transfer integral of TIPS-P is not only affected by the molecular packing parameters, but also by the nodal structure of frontier molecular orbitals, as visualized earlier in the case of sexithienyl.[41] For either a brick-wall packing structure of TIPS-P or a herring-bone packing structure of trimethylsilyl-substituted quarterthiophene (4T-TMS), oscillation of transfer integrals as a function of molecular displacements along the long and short axes is complicated. The multiscale theoretical approach presented in this work for elucidating the lattice strain, molecular packing, and charge carrier mobility relationship is applicable and easily extendable to other highly interested molecular materials, such as 4T-TMS and 2,7-dioctyl[1]benzothieno[3,2-b][1]benzothiophene (C$_8$-BTBT). The highly aligned C$_8$-BTBT thin-films grown by an off-centre spin-coating method in solution with hole mobility up to 43 cm^2 V^{-1} s^{-1} has been recently reported.[42] We believe that a prerequisite knowledge of the structure-property relationship is useful and will lead to an efficient and targeted control of the molecular packing and charge transport properties of these materials.

Supporting Information

Supporting Information is available from the Wiley Online Library or from the author. It includes details about the mobility calculation, the molecular packing parameters ($d_{\pi-\pi}$, d_{long} and d_{short}) of representative lattice-strained TIPS-P crystals, the unit-cell parameters and intermolecular transfer integrals of all 272 lattice-strained TIPS-P crystals investigated in this work.

[1] E. J. Meijer, D. M. de Leeuw, S. Setayesh, E. van Veenendaal, B. H. Huisman, P. W. M. Blom, J. C. Hummelen, U. Scherf, T. M. Klapwijk, *Nat. Mater.* **2003**, *2*, 678.

[2] G. H. Gelinck, H. E. A. Huitema, E. van Veenendaal, E. Cantatore, L. Schrijnemakers, J. B. P. H. van der Putten, T. C. T. Geuns, M. Beenhakkers, J. B. Giesbers, B.-H. Huisman, E. J. Meijer, E. M. Benito, F. J. Touwslager, A. W. Marsman, B. J. E. van Rens, D. M. de Leeuw, *Nat. Mater.* **2004**, *3*, 106.

[3] H. Sirringhaus, *Adv. Mater.* **2005**, *17*, 2411.

[4] J. E. Anthony, *Angew. Chem. Int. Ed.* **2008**, *47*, 452.

[5] S. Allard, M. Forster, B. Souharce, H. Thiem, U. Scherf, *Angew. Chem. Int. Ed.* **2008**, *47*, 4070.

[6] D. Kwak, J. A. Lim, B. Kang, W. H. Lee, K. Cho, *Adv. Funct. Mater.* **2013**, *23*, 5224.

[7] A. N. Sokolov, Y. Cao, O. B. Johnson, Z. Bao, *Adv. Funct. Mater.* **2012**, *22*, 175.

[8] Z. He, J. Chen, Z. Sun, G. Szulczewski, D. Li, *Org. Electron.* **2012**, *13*, 1819.

[9] J. Chen, C. K. Tee, M. Shtein, J. Anthony, D. C. Martin, *J. Appl. Phys.* **2008**, *103*, 114513.

[10] T. Kushida, T. Nagase, H. Naito, *Org. Electron.* **2011**, *12*, 2140.

[11] G. J. Chae, S.-H. Jeong, J. H. Baek, B. Walker, C. K. Song, J. H. Seo, *J. Mater. Chem. C* **2013**, *1*, 4216.

[12] D. K. Hwang, C. Fuentes-Hernandez, J. D. Berrigan, Y. Fang, J. Kim, W. J. Potscavage, H. Cheun, K. H. Sandhage, B. Kippelen, *J. Mater. Chem.* **2012**, *22*, 5531.

[13] W.-Y. Lee, J. H. Oh, S.-L. Suraru, W.-C. Chen, F. Würthner, Z. Bao, *Adv. Funct. Mater.* **2011**, *21*, 4173.

[14] G. Giri, E. Verploegen, S. C. B. Mannsfeld, S. Atahan-Evrenk, D. H. Kim, S. Y. Lee, H. A. Becerril, A. Aspuru-Guzik, M. F. Toney, Z. Bao, *Nature* **2011**, *480*, 504.

[15] Y. Diao, B. C. K. Tee, G. Giri, J. Xu, D. H. Kim, H. A. Becerril, R. M. Stoltenberg, T. H. Lee, G. Xue, S. C. B. Mannsfeld, Z. Bao, *Nat. Mater.* **2013**, *12*, 665.

[16] T. Sakanoue, H. Sirringhaus, *Nat. Mater.* **2010**, *9*, 736.

[17] C. Wang, D. Hwang, Z. Yu, K. Takei, J. Park, T. Chen, B. Ma, A. Javey, *Nat. Mater.* **2013**, *12*, 899.

[18] T. Someya, T. Sekitani, S. Iba, Y. Kato, H. Kawaguchi, T. Sakurai, *Proc. Natl. Acad. Sci. USA* **2004**, *101*, 9966.

[19] J. A. Rogers, T. Someya, Y. Huang, *Science* **2010**, *327*, 1603.

[20] S. C. B. Mannsfeld, B. C. K. Tee, R. M. Stoltenberg, C. V. H.-H. Chen, S. Barman, B. V. O. Muir, A. N. Sokolov, C. Reese, Z. Bao, *Nat. Mater.* **2010**, *9*, 859.

[21] K. Takei, T. Takahashi, J. C. Ho, H. Ko, A. G. Gillies, P. W. Leu, R. S. Fearing, A. Javey, *Nat. Mater.* **2010**, *9*, 821.

[22] B. C. K. Tee, C. Wang, R. Allen, Z. Bao, *Nat. Nanotechnol.* **2012**, *7*, 825.

[23] S. Plimpton, *J. Comput. Phys.* **1995**, *117*, 1.

[24] J. Wang, R. M. Wolf, J. W. Caldwell, P. A. Kollman, D. A. Case, *J. Comput. Chem.* **2004**, *25*, 1157.

[25] M. J. Frisch, G. W. Trucks, H. B. Schlegel, G. E. Scuseria, M. A. Robb, J. R. Cheeseman, G. Scalmani, V. Barone, B. Mennucci, G. A. Petersson, H. Nakatsuji, M. L. Caricato, X. Li, H. P. Hratchian, A. F. Izmaylov, J. Bloino, G. Zheng, J. L. Sonnenberg, M. Hada, M. Ehara, K. Toyota, R. Fukuda, J. Hasegawa, M. Ishida, T. Nakajima, Y. Honda, O. Kitao, H. Nakai, T. Vreven, J. Montgomery, J. A. Montgomery Jr., J. E. Peralta, F. Ogliaro, M. Bearpark, J. J. Heyd, E. Brothers, K. N. Kudin, V. N. Staroverov, R. Kobayashi, J. Normand, K. Raghavachari, A. Rendell, J. C. Burant, S. S. Iyengar, J. Tomasi, M. Cossi, N. Rega, N. J. Millam, M. Klene, J. E. Knox, J. B. Cross, V. Bakken, C. Adamo, J. Jaramillo, R. Gomperts, R. E. Stratmann, O. Yazyev, A. J. Austin, R. Cammi, C. Pomelli, J. W. Ochterski, R. L. Martin, K. Morokuma, V. G. Zakrzewski, G. A. Voth, P. Salvador, J. J. Dannenberg, S. Dapprich, A. D. Daniels, Ö. Farkas, J. B. Foresman, J. V. Ortiz, J. Cioslowski, D. J. Fox, Gaussian, Inc., Wallingford CT, **2009**.

[26] C. I. Bayly, P. Cieplak, W. Cornell, P. A. Kollman, *J. Phys. Chem.* **1993**, *97*, 10269.

[27] W. D. Cornell, P. Cieplak, C. I. Bayly, P. A. Kollmann, *J. Am. Chem. Soc.* **1993**, *115*, 9620.

[28] S. Nosé, *J. Chem. Phys.* **1984**, *81*, 511.

[29] W. G. Hoover, *Phys. Rev. A* **1985**, *31*, 1695.

[30] O. Kwon, V. Coropceanu, N. E. Gruhn, J. C. Durivage, J. G. Laquindanum, H. E. Katz, J. Cornil, J.-L. Brédas, *J. Chem. Phys.* **2004**, *120*, 8186.

[31] R. S. Sánchez-Carrera, V. Coropceanu, D. A. da Silva Filho, R. Friedlein, W. Osikowicz, R. Murdey, C. Suess, W. R. Salaneck, J.-L. Brédas, *J. Phys. Chem. B* **2006**, *110*, 18904.

[32] M. Malagoli, J.-L. Brédas, *Chem. Phys. Lett.* **2000**, *327*, 13.

[33] V. Lemaur, D. A. da Silva Filho, V. Coropceanu, M. Lehmann, Y. Geerts, J. Piris, M. G. Debije, A. M. van de Craats, K. Senthilkumar, L. D. A. Siebbeles, J. M. Warman, J.-L. Brédas, J. Cornil, *J. Am. Chem. Soc.* **2004**, *126*, 3271.

[34] E. F. Valeev, V. Coropceanu, D. A. da Silva Filho, S. Salman, J.-L. Brédas, *J. Am. Chem. Soc.* **2006**, *128*, 9882.

[35] H. Geng, Q. Peng, L. Wang, H. Li, Y. Liao, Z. Ma, Z. Shuai, *Adv. Mater.* **2012**, *24*, 3568.

[36] G. Nan, X. Yang, L. Wang, Z. Shuai, Y. Zhao, *Phys. Rev. B* **2009**, *79*, 115203.

[37] S. H. Lin, C. H. Chang, K. K. Liang, R. Chang, Y. J. Shiu, J. M. Zhang, T. S. Yang, M. Hayashi, F. C. Hsu, *Adv. Chem. Phys.* **2002**, *121*, 1.

[38] K. Asadi, A. J. Kronemeijer, T. Cramer, L. Jan Anton Koster, P. W. M. Blom, D. M. de Leeuw, *Nat. Commun.* **2013**, *4*, 1710.

[39] A. Krishnan, E. Dujardin, T. W. Ebbesen, P. N. Yianilos, M. M. J. Treacy, *Phys. Rev. B* **1998**, *58*, 14013.

[40] J. U. Lee, D. Yoon, H. Cheong, *Nano Lett.* **2012**, *12*, 4444.

[41] J. L. Brédas, J. P. Calbert, D. A. da Silva Filho, J. Cornil, *Proc. Natl. Acad. Sci. USA* **2002**, *99*, 5804.

[42] Y. Yuan, G. Giri, A. L. Ayzner, A. P. Zoombelt, S. C. B. Mannsfeld, J. Chen, D. Nordlund, M. F. Toney, J. Huang, Z. Bao, *Nat. Commun.* **2014**, *5*, 3005.